STUDYING DEFORMATION OF VOLCANOES IN THE ALEUTIAN ISLANDS USING L-BAND ALOS PALSAR INTERFEROMETRY

Proposal ID: 057

PI: Zhong Lu[(1)]
Co-PIs: Daniel Dzurisin[(1)], Charles Wicks Jr.[(2)], and John Power[(3)]

[(1)] U.S. Geological Survey, 1300 SE Cardinal Court, Vancouver, WA 98683, USA.; E-mail:lu@usgs.gov, dzurisin@usgs.gov
[(2)] U.S. Geological Survey, 345 Middlefield Rd., Menlo Park, CA 94025, USA; E-mail:cwicks@usgs.gov
[(3)] U.S. Geological Survey, 4200 University Drive, Anchorage, AK 99508, USA; jpower@usgs.gov

Abstract

We have mapped ground surface deformation associated volcanic events at Aleutian volcanoes using JERS-1 and ALOS PALSAR images. The derived surface deformation measurements have enabled the construction of detailed numerical models to study magmatic processes. We have demonstrated that InSAR deformation imagery and derived deformation models are critical in understanding the magma plumbing system over Aleutian and volcanism in the world.

1. INTRODUCTION

The Aleutian arc contains about 8% of the world's active volcanoes and more than 85 percent of historically active volcanoes in U.S. During the past decade, there has been an average of 3 - 4 eruptions per year in the arc. Aleutian volcanoes span the entire spectrum in eruptive style, size, volume, and magma composition.

In general, the "eruption cycle" of a volcano can be conceptualized as a series of events from deep magma generation to surface eruption, including such stages as partial melting, initial ascent through the upper mantle and lower crust, crustal assimilation, magma mixing, degassing, shallow storage, and finally ascent to the surface [1, 2]. This process is complex, varying from one eruption to the next and from volcano to volcano. In many cases, volcanic eruptions are preceded by pronounced ground deformation in response to increasing pressure from magma chambers or the upward intrusion of magma [3]. Therefore, surface deformation imagery from interferometric synthetic aperture radar (InSAR) can provide important insights into the structure, plumbing, and state of restless volcanoes. Surface deformation can be the first sign of increasing levels of volcanic activity, preceding swarms of earthquakes or other precursors that signal impending intrusions or eruptions.

We have proposed to apply InSAR technique to study and monitor ground surface deformation at active and remote volcanoes in the Alaska-Aleutian arc using L-band JERS-1 and ALOS PALSAR images. We would like to 1) measure ground deformation at several Aleutian volcanoes using repeat-pass interferometric JERS-1 and PALSAR images; 2) model the observed deformation to study the process of volcanic plumbing systems using different deformation sources; 3) provide the scientific inputs to the relevant agencies to facilitate the monitoring efforts at these volcanoes. The proposed research compliments our efforts on monitoring these volcanoes using ERS-1/-2, Radarsat-1, Envisat, and TerraSAR-X SAR images. Our goal was to monitor the deformation during the entire eruption cycle (one decade or two) at these volcanoes, using the ERS-1, JERS-1, Radarsat-1, ERS-2, ENVISAT, TerraSAR-X and ALOS satellites. We seek to understand the deformation patterns of each volcano, to be better prepared to deal with future eruptions. Because the selected targets are analogues to the great majority of the world's hazardous volcanoes, our results will have broad applicability to the many similar volcanoes in Japan and the worldwide.

2. METHODS

We have used a 1-arc-second digital elevation model (DEM) from the Shuttle Radar Topography Mission to create deformation interferograms from suitable pairs of SAR images. Both conventional 2-pass InSAR processing [4] and advanced InSAR

processing techniques (see below) have been exploited to improve the quality of the deformation maps.

2.1 InSAR processing: improved technique for long baseline InSAR image

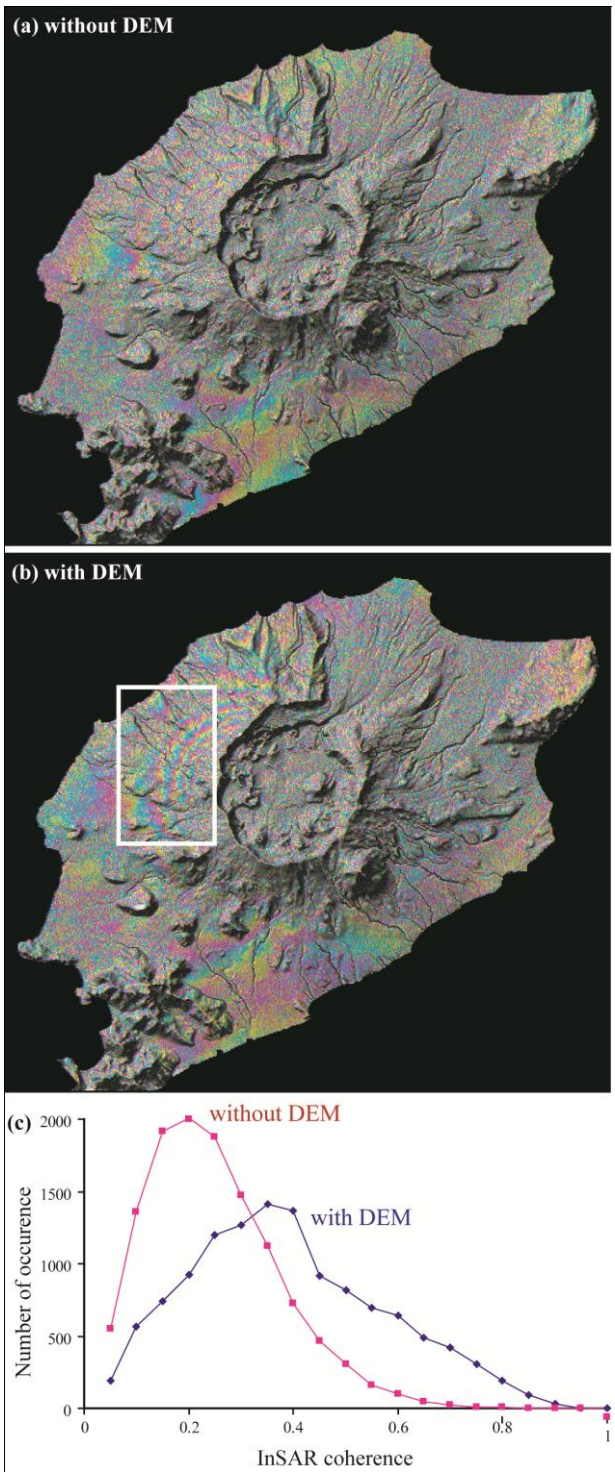

Figure 1. ALOS PALSAR Interferograms of Okmok volcano formed (*a*) with and (*b*) without taking into account the effect of topography during image registration and re-sampling of the SAR images. (*c*) Histograms of InSAR coherence within the area outlined by the white rectangle in (*b*). Rightward shift of the distribution maximum for the interferogram that includes topographic effects (blue line) relative to the uncorrected interferogram (red line) indicates the coherence improvement by ~0.2 in the corrected interferogram.

A stringent prerequisite in InSAR processing is the precise registration of reference and slave SAR images and re-sampling the slave image to the geometry of the reference image. For conventional InSAR processing, co-registration is done by cross-correlating the reference and slave images at a dense grid of pixel locations and using the results to construct range and azimuth offset polynomials for the entire image. The range and azimuth offset polynomials are expressed as functions of range and azimuth pixel position. A problem arises when, for an interferogram with a large perpendicular baseline, topographic variations introduce additional localized offsets between the reference and slave images. The range offset due to topographic relief is linearly dependent on topography and can be approximated as [5]:

$$\Delta r_{off} = -\frac{B_{\perp}}{H \tan\theta}\Delta h \qquad (1)$$

where Δr_{off} is the range offset due to height difference Δh, $B_{\perp}$ is the perpendicular baseline of the interferogram, H is the altitude of the satellite above Earth, and θ is the SAR look angle. For the ALOS PALSAR sensor, normal values for H and θ are about 700 km and 34°, respectively. The topography-induced range offset for a fine-beam PALSAR interferogram with a perpendicular baseline of 1 km can be as large as ~2.1 m, or about 23% of the range pixel size. In other words, range offsets due to topographic relief at Okmok can be large enough to degrade InSAR coherence if the offsets are not taken into account during image co-registration. We have used a DEM and the SAR imaging geometry to compute direct functions that map the position of each pixel in the reference image to a corresponding pixel location in the slave image. This results in significant improvement in coherence for interferograms with relatively large baselines [5].

To illustrate the improvement in InSAR coherence obtained by accounting for topography-induced range offsets, we used an ALOS PALSAR interferogram with a perpendicular baseline of 3876 m (Figure 1). Topographic relief of 1 km produces a range shift of about 8 m for a baseline of this length. We compared an unfiltered interferogram produced using conventional InSAR processing (Figure 1*a*) with an unfiltered interferogram that takes into

account the range offset due to topography (Figure 1*b*). Improved coherence in the second case is evidenced by better defined interferometric fringes on Okmok's western flank, and by a coherence histogram for that area (Figure 1*c*).

2.2 Multiple aperture InSAR (MAI)

The conventional approach to measuring along-track displacements near the deformation center is to use image correlation to map the pixel offset field, which can be done to an accuracy of about 1/10 of the pixel size (~5 m). Bechor and Zebker [6] introduced a multiple aperture InSAR (MAI) technique, which was then improved by Jung et al. [7], to produce along-track displacement images that represent a remarkable improvement over the pixel offset tracking method. MAI utilizes sub-aperture processing techniques to create one forward-looking single-look-complex (SLC) image and one backward-looking SLC image from raw SAR data. Two raw SAR datasets processed in this way are used to form one forward-looking and one backward-looking interferogram from the corresponding SLC images. The phase difference between the forward-looking and backward-looking interferograms is an MAI image that shows ground surface displacements in the azimuth (*i.e.*, along-track) direction, which is approximately north-south for all operational SAR satellites.

We applied MAI processing to InSAR images that bracket the 1997 and 2008 eruptions at Okmok volcano to prospect for along-track surface deformation associated with rifting or dike opening, which commonly occurs during effusive eruptions. In the center of the caldera where coherence was maintained, the MAI image indicates no significant north-south surface displacement during the 1997 and 2008 eruptions [5]. Therefore, we surmise that the 1997 and 2008 eruptions were not fed from a cross-caldera dike or fissure system, but rather from a localized vent or vents along the caldera's ring fracture system.

2.3 3-D deformation mapping by combing InSAR and MAI images

InSAR technique is limited to measurement of displacements along the radar line–of-sight (LOS) direction. Because SAR satellites have near-polar orbits (i.e., approximately N-S ground tracks and E-W look directions), it is impossible to determine three-dimensional (3D) surface deformation from LOS InSAR data alone. When deformation magnitudes are on several tens of centimeters, it is possible to reconstruct the 3D deformation field from InSAR using two interferograms generated from ascending and descending pairs and one or two azimuth pixel offset tracking fields created by cross correlation of SAR images. This method has difficulty in determining the north component of surface deformation due to the low sensitivity of the SAR pixel offset tracking method (relative to LOS displacement resolution).

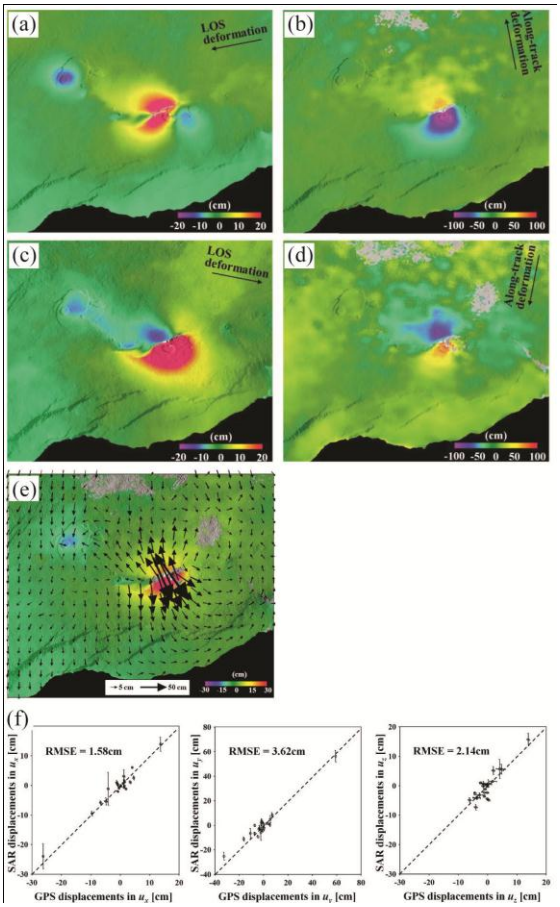

Figure 2. (a-d) LOS and along-track surface deformation fields of the June 2007 eruption at Kilauea volcano constructed from (a, b) InSAR and MAI interferograms of ALOS PALSAR ascending pair acquired on 5 May 2007 and 20 June 2007 and (c, d) InSAR and MAI interferograms of ALOS PALSAR descending pair acquired on 28 February 2007 and 16 July 2007. (e) 3D surface deformation field based on two LOS and two along-track MAI images. (f) Comparison of 3D deformation measurements estimated from ALOS InSAR/MAI techniques with GPS displacements at 24 stations on Kilauea Volcano for the east, north, and up components. Circles and bars denote uncertainties of InSAR/MAI and GPS measurements at 2 standard deviations, respectively [8].

Because MAI technique represents a remarkable improvement in measuring along-track deformation than the pixel offset tracking method, we have developed a technique on constructing 3D deformation field by integrating MAI technique and conventional InSAR using one (or more)

descending and one (or more) ascending interferogram pairs [8].

Let $d = (d_x, d_y, d_z)^{\mathbf{T}}$ be the 3D deformation vector in a local (east, north, up) reference frame, and $u = (u_x, u_y, u_z)^{\mathbf{T}}$ be the unit LOS deformation or along-track deformation vector expressed in the same local reference frame. If u is the LOS deformation vector, $u = (-\sin\theta \cdot \cos\varphi, \sin\theta \cdot \sin\varphi, \cos\theta)^{\mathbf{T}}$, where θ is the radar incidence from vertical and φ is satellite track angles from north of the LOS vector, respectively. Calculations of the θ and φ are performed on a pixel-by-pixel basis. If u is the along-track deformation vector, $u = (-\sin\varphi, -\cos\varphi, 0)^{\mathbf{T}}$. The deformation, *r*, measured from an InSAR or MAI is given by:

$$r = -u^{\mathbf{T}} d \qquad (2)$$

Suppose we produce a total of *n* InSAR and MAI interferograms (observations), then we obtain $R = (r_1, r_2, ..., r_n)^{\mathbf{T}}$. The weighted least-squares solution ($\hat{d}$) for *d* is defined as follows:

$$\hat{d} = -\left(U^{\mathbf{T}} \boldsymbol{\Sigma}^{-1} U\right)^{-1} \cdot \left(U^{\mathbf{T}} \boldsymbol{\Sigma}^{-1} R\right) \qquad (3)$$

where $\boldsymbol{\Sigma}$ is the covariance matrix for errors in the observed deformation observations, U and R are given by $U = (u_1, u_2, u_3 ..., u_n)^{\mathbf{T}}$ and $R = (r_1, r_2, r_3 ..., r_n)^{\mathbf{T}}$, respectively.

In the case that we assume the covariance matrix as a diagonal matrix, we get $\boldsymbol{\Sigma} = \mathrm{diag}(\sigma_1^2, \sigma_2^2, \sigma_3^2, ..., \sigma_n^2)$, where diag(·) denotes a diagonal matrix. To determine the relative weighting factors for the InSAR and MAI measurements, we estimate the corresponding standard deviations in the InSAR and MAI images [8].

The power of this 3D construction method has been demonstrated by applying this technique to the June 17–19, 2007, intrusion and eruption along the East Rift Zone of Kilauea Volcano, Hawaii [8]. The radar-measured 3D surface deformation agrees with GPS data from 24 sites on the volcano, and the root mean square errors in east, north and up components of displacement are 1.6, 3.6 and 2.1 cm, respectively (Figure 2). The remarkable improvement of accuracy in the north component over other techniques is primarily due to the improved deformation measurement in the N-S direction by MAI technique [8]. We believe that 3D deformation mapping by combining InSAR and MAI techniques will provide data that can result in improved deformation source models for various applications.

3. RESULTS

The following section highlights a few examples of our results and accomplishments based on JERS-1 and ALOS InSAR deformation images along with ERS-1/-2, Envisat and Radarsat-1 InSAR imagery and derived deformation models.

3.1 Akutan

In March 1996, an intense earthquake swarm beneath Akutan Island, Alaska, was accompanied by extensive ground cracking but no eruption of Akutan volcano. Radar interferograms produced from L-band JERS-1 and C-band ERS-1/2 images show uplift by as much as 60 cm on the western part of the island associated with the swarm (Figure 3) [9]. The JERS interferograms have greater coherence, especially in areas with loose surface material or thick vegetation. They also show subsidence of similar magnitude on the eastern part of the island, plus displacements along faults reactivated during the swarm. The axis of uplift and subsidence strikes about N70°W, which is roughly parallel to a zone of fresh cracks on the volcano's northwest flank, to normal faults that cut the island, and to the inferred maximum compressive stress direction. A common feature of models that fit the deformation is the emplacement of a shallow dike along this trend beneath the volcano's northwest flank. Both before and after the swarm, the northwest flank was uplifted 5-20 mm/year relative to the southwest flank, probably by magma intrusion. The zone of fresh cracks subsided about 20 mm during 1996-1997 and at lesser rates thereafter, possibly because of cooling and degassing of the intrusion [9].

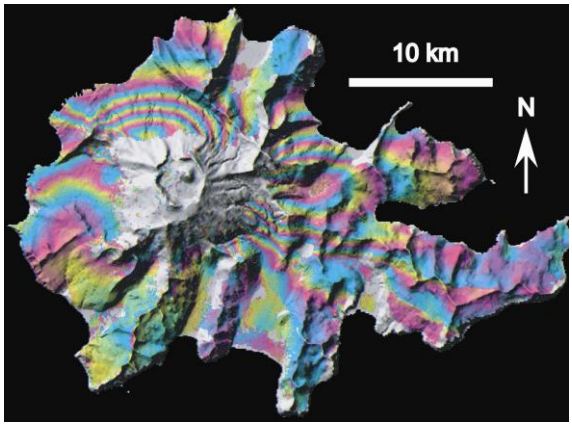

Figure 3. A deformation interferogram of Akutan Island, constructed from L-band JERS-1 SAR images for the period from 28 October 1994 to 22 June 1997, showing uplift of the west half of the island and subsidence of the east half during the 1996 seismic swarm. Each fringe (full color cycle)

represents 11.76 cm range change in the satellite look direction. Areas that lack interferometric coherence are uncolored.

3.2 Okmok

We have used L-band and C-band InSAR images to study transient deformation of Okmok volcano before, during, and after the 1997 eruption (Figure 4). The volcano inflated at a generally declining rate prior to its 1997 eruption, deflated rapidly during the eruption, and resumed inflating several months thereafter at a rate that varied over time from summer 1997 to 10 July 2008 before the 2008 eruption [5, 10-12]. Inversion of the surface deformation data shows that the horizontal position of the center of a magma storage zone that underlies Okmok Caldera at ~3.0 km below sea level remained nearly stationary from 1992 to 2008. InSAR images show that the maximum surface uplift rate prior to either eruption was ~20 cm/yr during 2002–2003; minimum inflation rates of 2–5 cm/year occurred during 1993–1995 and 2005–2006. Subsidence of a few centimeters was observed during 1995–1996 before the 1997 eruption, and also during 2004–2005 before the 2008 eruption. We propose that the supply rate decreased in response to the diminishing pressure gradient between the shallow storage zone and a deeper magma source region. Eventually the effects of continuing magma supply and vesiculation of stored magma caused a critical pressure threshold to be exceeded, triggering the 2008 eruption. A similar pattern of initially rapid inflation followed by oscillatory but generally slowing inflation was observed prior to the 1997 eruption. In both cases, withdrawal of magma during the eruptions depressurized the shallow storage zone, causing significant volcano-wide subsidence and initiating a new inter-eruption deformation cycle.

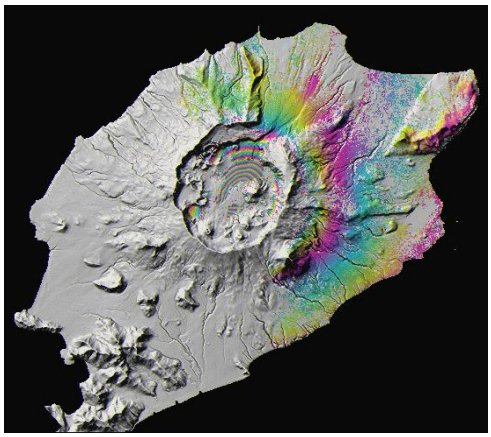

Figure 4. A JERS-1 interferogram showing volcanic deflation associated with the 1997 eruption at Okmok volcano, Alaska. Each fringe (full color cycle) represents 11.8 cm of range change between the ground and the satellite. The interferogram covers an area of 44 km by 39 km. Areas that lack interferometric coherence are uncolored.

A hydrovolcanic eruption near Cone D on the floor of Okmok Caldera, Alaska, began on 12 July 2008 and continued until late August 2008. We have used ALOS PALSAR, Envisat, ERS-2 and Radarsat-1 data to produce a suite of 2008 co-eruption deformation maps [5]. Most of the surface deformation that occurred during the eruption is explained by deflation of a Mogi-type source located beneath the center of the caldera and 2–3 km below sea level, *i.e.*, essentially the same source that inflated prior to the eruption. During the eruption the reservoir deflated at a rate that decreased exponentially with time with a 1/*e* time constant of ~13 days. We envision a sponge-like network of interconnected fractures and melt bodies that, in aggregate, constitute a complex magma storage zone beneath Okmok Caldera. The rate at which the reservoir deflates during an eruption may be controlled by the diminishing pressure difference between the reservoir and surface. A similar mechanism might explain the tendency for reservoir inflation to slow as an eruption approaches, until the pressure difference between a deep magma production zone and the reservoir is great enough to drive an intrusion or eruption along the caldera ring-fracture system.

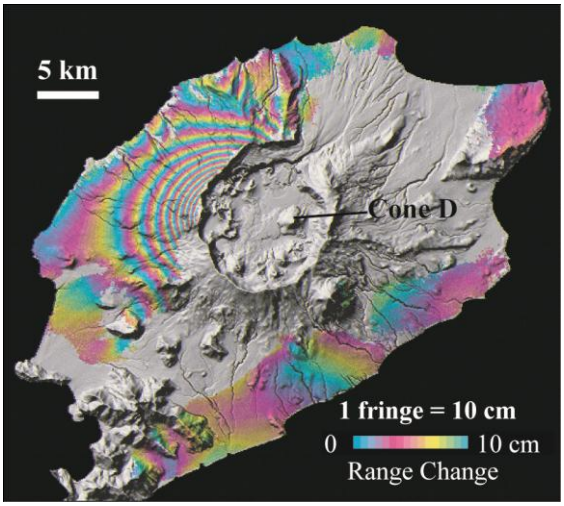

Figure 5. An example of interferograms that span the 2008 eruption at Okmok volcano (Lu and Dzurisin, 2010). This InSAR image is based on PALSAR images acquired on August 22, 2007 - October 7, 2008. One fringe (color cycle) represents 10 cm of line-of-sight (LOS) ground motion in all cases. Areas that lack interferometric coherence are uncolored.

We have also mapped the deformation of lava flows after emplacement (Figure 6). To explain persistent subsidence of the 1997 lava flow, Lu et al. [11]

considered three possible mechanisms: 1) poroelastic deformation of the caldera floor caused by the lava-flow gravity load; 2) thermoelastic deformation of the flow due to cooling after emplacement; and 3) viscoelastic relaxation of the caldera floor caused by the lava-flow gravity load [13, 14]. Lu et al. [11] constructed two-dimensional finite element models of the deformation field for each mechanism, and concluded that the subsidence most likely was caused by a combination of thermoelastic cooling of the 1997 flow and viscoelastic relaxation of the caldera floor in response to the gravity load from both the 1997 and nearby pre-1997 flows.

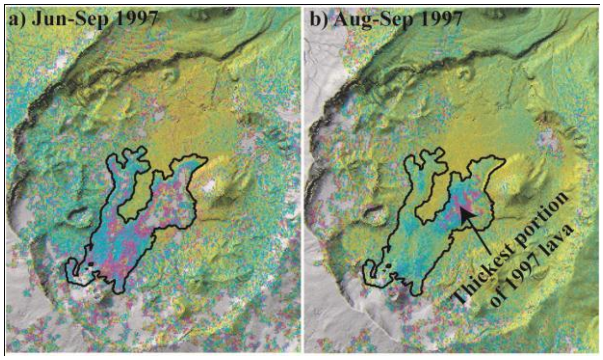

Figure 6. JERS-1 interferograms showing post-emplacement surface movement of 1997 lava flows a few months after the 1997 eruption. Surface displacement due to lava contraction reached 2 mm/day around 4 months after the emplacement. One fringe (a full color cycle) represents 11.8 cm of range change along the satellite's look direction. The extent of 1997 lava flows is outlined. Areas that lack interferometric coherence are uncolored. The thickest portion of the 1997 lava flows is marked.

The effect of lava flow contraction can last many years [11, 12]. For example, a significant amount of subsidence (1 to 2 cm/year) has been observed about 50 years after the emplacement of the 1958 lava flows at Okmok volcano [11, 12]. This has cautionary implications for positioning geodetic markers and deformation sensors at Okmok and other similar volcanoes, and for interpretation of resulting point-measurement data (*e.g.*, GPS, tilt, borehole strain). InSAR images can provide an important spatial context for such endeavors, thus helping to avoid misinterpretations caused by unrecognized deformation sources such as young flows, localized faulting, or hydrothermal activity.

3.3 Volcanoes with frequent eruptions

Cleveland Volcano, a stratovolcano in the central-western Aleutian arc, is frequently observed emitting steam and ash. Most of the activity is characterized as profuse steaming from the summit crater with intermittent emissions of ash and occasional debris flows. Numerous minor explosive eruptions occurred since 2001. Figure 3 is a 92-day L-band ALOS InSAR image spanning July 27 and October 27, 2007, when several minor eruptions occurred (Figure 7). No significant volcano-wide deformation was observed over the volcano flank. Note the L-band InSAR image could not maintain coherence over the snow-covered summit and upper flank of Cleveland volcano.

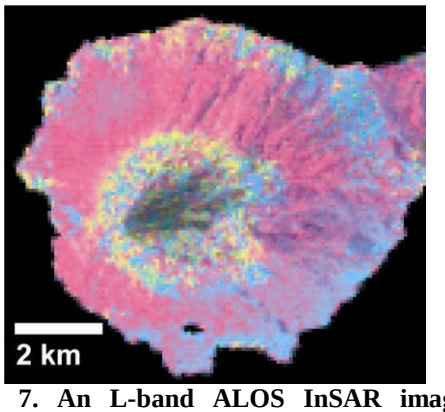

Figure 7. An L-band ALOS InSAR image of Cleveland volcano spanning July-Oct. 2007, showing loss of coherence over the snow-covered summit and no significant deformation over the flank of Cleveland.

Pavlof Volcano is approximately 7 km in base diameter and has active vents on the north and east sides, close to the summit. Pavlof is the most active volcano in the Aleutian arc with almost 40 relatively well-documented eruptions dating back to 1790. Pavlof eruptions are typically strombolian to vulcanian in character and consist of the rhythmic ejection of incandescent bombs and ash. Figure 4 shows an ALOS image acquired during July 31 and September 15, 2007, spanning the August 2007 eruption (Figure 8). No significant volcano-wide was observed over the flank of the Pavlof volcano where InSAR coherence is maintained. Note the loss of L-band InSAR coherence over the snow-covered summit of Pavlof volcano.

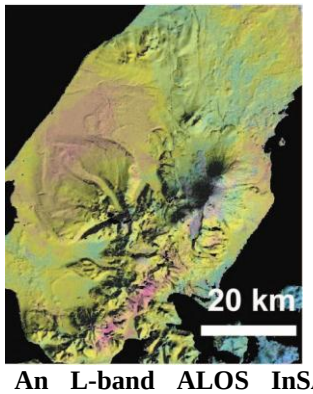

Figure 8. An L-band ALOS InSAR image bracketing the Aug. 2007 eruption, showing loss of coherence over the snow-covered summit and no significant deformation over the flank of Pavlof.

The frequently active volcanoes over Aleutians, such as Pavlof and Cleveland, exhibit little or no measurable deformation [15]. They all are stratovolcanoes, have symmetric cones, and erupt frequently. Interferograms that span time intervals before, during, and after recent eruptions do not show any significant deformation. Plausible explanations include the following: 1) pre-eruptive inflation is balanced by co-eruptive deflation, resulting in little or no net deformation; 2) the magma reservoirs are deep, so inflation or deflation causes only broad, subtle deformation of the surface that is difficult to detect, especially if the area of radar coherence is limited; 3) no significant pre-eruptive and co-eruptive deformation is associated with these eruptions; and 4) the magma reservoir is very shallow and its strength is small (i.e., pressure or volume changes in the reservoir are small), so deformation only occurs over a small area (a few km in radius) near the summit where coherence is lost owing to perennial ice or snow [15, 16]. Further study requires better temporal sampling than is available from current SAR satellites and an L-band sensor to defeat interferometric decorrelation due to snow/ice cover. Better monitoring of this type of volcano also requires observations from continuous GPS and seismometers to capture localized or short-term deformation, if it exists.

3.4 INSAR coherence

We have compared InSAR coherence between L-band and C-band interferograms over Aleutians. As expected, we have found that the L-band interferogram maintained much higher coherence than the C-band one, particularly at vegetated areas. The higher coherence is mainly due to the relatively longer wavelength and larger bandwidth of the L-band ALOS PALSAR.

The reduction of InSAR coherence is the major obstacle to applying InSAR on Aleutian volcanoes. At Aleutian volcanoes, processes that reduce interferometric coherence include snow/ice melting and accumulation, freezing/thawing of surface material, erosion/deposition of volcanic lava and ash, and dense vegetation. Therefore, the best chance of producing coherent interferograms is to use images acquired during summer or early fall, separated in time by one to a few years. We have shown that L-band InSAR images that span more than 1 month do not maintain coherence over the snow or glacier covered summits of Aleutian volcanoes. To obtain coherent interferograms for reliably near-real time monitoring of restless volcanoes in sub-arctic environment, future satellite passes must be made at least 2-3 days for the C-band radar and less than 1 week for L-band radar during winters.

4. CONCLUSION

JERS-1 and ALOS PALSAR imagery has played a critical role in our studies of volcanic deformation at Aleutian volcanoes. The L-band InSAR images, along with C-band data from other sensors, have allowed us to explore various models to understand the mechanism that caused the surface deformation and helped us better understand how these volcanoes work.

Acknowledgements. ALOS SAR data are copyrighted by JAXA/METI. JERS-1 SAR images are copyrighted JAXA/MITI. Both ALOS PALSAR and JERS-1 SAR raw data were provided by ASF and JAXA through AO 057. We thank JAXA and ASF for their outstanding support in making SAR data available to us on a timely basis, H.S. Jung for help with MAI processing, and C.W. Lee for assistance in exploring ALOS PALSAR InSAR images over Aleutians.

REFERENCES

[1] D., Dzurisin, "A comprehensive approach to monitoring volcano deformation as a window on eruption cycle", *Rev. Geophys., Review of Geophysics*, *41*, 10.1029/2001RG000107, 2003.

[2] D. Dzurisin, "*Volcano Deformation – Geodetic Monitoring Techniques"*, 441 pp., Springer-Praxis Publishing Ltd, Chichester, UK, 2007.

[3] J. Dvorak, and D. Dzurisin, "Volcano geodesy: The search for magma reservoirs and the formation of eruptive vents", *Rev. Geophys., 35*, 343-384, 1997.

[4] D., Massonnet, and K. Feigl, "Radar interferometry and its application to changes in the Earth's surface", *Rev. Geophys., 36*, 441-500, 1998.

[5] Z. Lu, and D. Dzurisin, "Ground surface deformation patterns, magma supply, and magma storage at Okmok volcano, Alaska, inferred from InSAR analysis: 2. Co-eruptive deflation, July-August 2008", *Journal of Geophysical Research*, 115, B00B02, doi:10.1029/2009JB006970, 2010.

[6] N. Bechor, and H. Zebker, "Measuring two-dimensional movements using a single InSAR pair", *Geophys. Res. Lett.*, 33, L16311, doi:10.1029/2006GL026883, 2006.

[7] H.S. Jung, J.S. Won, and S.W. Kim, "An improvement of the performance of multiple aperture SAR interferometry (MAI)", *IEEE Trans. Geosci. Remote Sens.*, 47, 2859-2969, 2009.

[8] H.S. Jung, Z. Lu, J.S. Won, M.P. Poland and A. Miklius, "Mapping three-dimensional surface deformation by combining multiple aperture interferometry and conventional interferometry: application to the June 2007 eruption at the Kilauea

volcano, Hawaii", *IEEE Geos. Rem. Sens. Lett.*, 8, 34-38, 10.1109/LGRS.2010.2051793, 2011.

[9] Z. Lu, C. Wicks, O. Kwoun, J. Power, and D. Dzurisin, "Surface deformation associated with the March 1996 earthquake swarm at Akutan Island, Alaska, revealed by C-band ERS and L-band JERS radar interferometry", *Canadian Journal of Remote Sensing*, 31, 7-20, 2005.

[10] Z. Lu, D. Mann, J. Freymueller, and D. Meyer, "Synthetic aperture radar interferometry of Okmok volcano, Alaska: Radar observations", *J. Geophys. Res*., *105*, 10791-10806, 2000.

[11] Z. Lu, T. Masterlark, and D. Dzurisin, "Interferometric Synthetic Aperture Radar (InSAR) Study of Okmok Volcano, Alaska, 1992-2003: Magma Supply Dynamics and Post-emplacement Lava Flow Deformation", *Journal of Geophysical Research*, 110, B02403, DOI:10.1029/2004JB003148, 2005.

[12] Z., Lu, D. Dzurisin, J. Biggs, C. Wicks, Jr, and S. McNutt, "Ground surface deformation patterns, magma supply, and magma storage at Okmok volcano, Alaska, inferred from InSAR analysis: 1. inter-eruptive deformation, 1997-2008", *Journal of Geophysical Research*, 115, B00B03, doi:10.1029/2009JB006969, 2010.

[13] P. Briole, D. Massonnet, and C. Delacourt, "Post-eruptive deformation associated with the 1986-87 and 1989 lava flows of Etna detected by radar interferometry", *Geophys. Res. Lett. 24*, 37-40, 1997.

[14] N. Stevens, G. Wadge, C. Williams, J. Morley, J.P. Muller, J.B. Murray, M. Upton, "Surface movements of emplaced lava flows measured by synthetic aperture radar interferometry", *J. Geophys. Res*., *106*, 11,293-11,313, 2001.

[15] Z. Lu, D. Dzurisin, C. Wicks, J. Power, O. Kwoun, and R. Rykhus, "Diverse deformation patterns of Aleutian volcanoes from satellite interferometric synthetic aperture radar (InSAR)", in Volcanism and Subduction: The Kamchatka Region (edited by J. Eichelberger et al.), *American Geophysical Union Geophysical Monograph Series 172*, p. 249-261, 2007.

[16] S. Moran, O. Kwoun, T. Masterlark, and Z. Lu, "On the absence of deformation signals from InSAR interferograms bracketing the 1995-1996 and 1999 eruptions of Shishaldin Volcano, Alaska", *Journal of Volcanology and Geothermal Research*, *150*, 119-131, 2006.

APPENDIX 1: ***PAPERS PUBLISHED UNDER THIS RESEARCH***

Journal papers & book chapters:

1. Lu, Z., C. Wicks, O. Kwoun, J. Power, and D. Dzurisin, Surface deformation associated with the March 1996 earthquake swarm at Akutan Island, Alaska, revealed by C-band ERS and L-band JERS radar interferometry, Canadian Journal of Remote Sensing, vol. 31, no. 1, 7-20, 2005.

2. Lu, Z., T. Masterlark, and D. Dzurisin, Interferometric Synthetic Aperture Radar (InSAR) Study of Okmok Volcano, Alaska, 1992-2003: Magma Supply Dynamics and Post-emplacement Lava Flow Deformation, Journal of Geophysical Research, vol. 110, no. B2, B02403, DOI:10.1029/2004JB003148, 2005.

3. Moran, S., O. Kwoun, T. Masterlark, and Z. Lu, On the absence of deformation signals from InSAR interferograms bracketing the 1995-1996 and 1999 eruptions of Shishaldin Volcano, Alaska, Journal of Volcanology and Geothermal Research, vol. 150, 119-131, 2006.

4. Lu, Z., D. Dzurisin, C. Wicks, J. Power, O. Kwoun, and R. Rykhus, Diverse deformation patterns of Aleutian volcanoes from satellite interferometric synthetic aperture radar (InSAR), in Volcanism and Subduction: The Kamchatka Region (edited by J. Eichelberger et al.), American Geophysical Union Geophysical Monograph Series 172, 249-261, 2007.

5. Lu, Z., InSAR Imaging of Volcanic Deformation Over Cloud-prone Areas—Aleutian Islands, Photogrammetric Engineering & Remote Sensing, 73, 3, 245-257, 2007.

6. Dzurisin, D., and Z. Lu, Interferometric Synthetic Aperture Radar (InSAR) (Chapter 5), in *Volcano Deformation: Geodetic Monitoring Techniques*, by D. Dzurisin, Springer-Praxis Publishing Ltd., UK, 2007.

7. Lu, Z., and Dzurisin, D., Ground surface deformation patterns, magma supply, and magma storage at Okmok volcano, Alaska, inferred from InSAR analysis: 2. Co-eruptive deflation, July-August 2008: Journal of Geophysical Research, 115, B00B02, doi:10.1029/2009JB006970, 2010.

8. Lu, Z., Dzurisin, D., Jung, H.S., Zhang, J.X., and Zhang, Y.H., Radar Image and Data Fusion for Natural Hazards Characterization: International Journal of Image and Data Fusion, 1, 217-242, 2010.

9. Lu, Z., Zhang, J., Zhang, Y., and Dzurisin, D., Monitoring and characterizing natural hazards with satellite InSAR imagery: Annals of GIS, 16, 55-66, 2010.

10. Lu, Z., Dzurisin, D., Biggs, J., Wicks, C., Jr, and McNutt, S., Ground surface deformation patterns, magma supply, and magma storage at Okmok volcano, Alaska, inferred from InSAR analysis: 1. inter-eruptive deformation, 1997-2008: Journal of Geophysical Research, 115, B00B03, doi:10.1029/2009JB006969, 2010.

11. Jung, H.S., Z. Lu, J.S. Won, M.P. Poland and A. Miklius, Mapping three-dimensional surface deformation by combining multiple aperture interferometry and conventional interferometry: application to the June 2007 eruption at the Kilauea volcano, Hawaii, *IEEE Geos. Rem. Sens. Lett.*, vol. 8, no. 1, 34-38, 10.1109/LGRS.2010.2051793, 2011.

12. Lu, Z., D. Dzurisin, C. Wicks, and J. Power, Interferometric Synthetic Aperture Radar (InSAR): a Long-Term Monitoring Tool, "Volcanoes of the North Pacific: Observations from Space", edited by K. Dean and J. Dehn, in press, 2011.

Proceeding papers & news articles:

1. Lu, Z., ALOS PALSAR InSAR, Alaska Satellite Facility News & Notes, vol. 4, no. 4, p. 1-2, 2007.

2. Lu, Z., D. Dzurisin, C. Wicks, and J. Power, Diverse Deformation Patterns Of Aleutian Volcanoes From InSAR, Proceedings of Fringe 2007 Workshop, Frascati, ESA, Nov 24-29, 2007.

3. Lu, Z., Monitoring and characterizing natural hazards with satellite InSAR imagery, Proceedings of ISPRS Symposium on Techniques and Applications of Optical and SAR Imagery Fusion, p. 57-67, Chengdu, China, 2007.

4. Lu, Z., Interferometric Synthetic Aperture Radar: Building Tomorrow's Tools Today, Alaska Satellite Facility News & Notes, 15th Anniversary Special Edition, p. 12-14, August 2006.

5. Lu, Z., InSAR imaging of Aleutian volcanoes, Proceedings of the 1st International symposium on cloud-prone and rainy areas remote sensing, edited by H. Lin et al., 283-297, The Chinese University of Hong Kong, Hong Kong, 2005.

6. Lu, Z., C. Wicks, D. Dzurisin, and J. Power, Studying Aleutian Volcanoes with InSAR, Alaska Satellite Facility News & Notes, vol. 1, no. 4, page 4-6, 2004.

7. Lu, Z., C. Wicks, D. Dzurisin, and J. Power, InSAR Studies of Alaska Volcanoes, Proceedings of International Symposium of Remote Sensing (ISRS), 2004.

APPENDIX 2: OTHER *PAPERS PUBLISHED UTILIZING ALOS PALSAR FROM ASF AND JAXA*

1. Kim, J., Z. Lu, H. Lee, C. Shum**,** C. Swarzenski, T. Doyle, S. Baek, Integrated Analysis of PALSAR/Radarsat-1 InSAR and ENVISAT altimeter for mapping of absolute water level changes in Louisiana wetland, *Remote Sensing of Environment*, doi:10.1016/j.rse.2009.06.014., 2009.

2. Lu, Z., J.W. Kim, H. Lee, C. Shum, J. Duan, M. Ibaraki, O. Akyilmaz, C. Read, Helmand River hydrologic studies using ALOS PALSAR InSAR and ENVISAT altimetry, *Marine Geodesy*, 32:3, 320–333, 10.1080/01490410903094833, 2009.

3. Lu, Z., and Kwoun, O., Interferometric synthetic aperture radar (InSAR) study of coastal wetlands over southeastern Louisiana: in Remote Sensing of Wetlands, edited by Y.Q. Wang, CRC Press, p. 25-60, 2009.

4. Lu, Z., and Wicks, C., Study of the 6 August 2007 Crandall Canyon mine (Utah, USA) collapse from ALOS PALSAR InSAR: Geomatics, Natural Hazards and Risk, Geomatics, Natural Hazards and Risk, 1, 85-93, 2010.

5. Pallister, J., McCausland, W., Jónsson, S., Lu, Z., Zahran, H., Hadidy, S., Aburukbah, A., Stewart, I., Lundgren, P., White, R., and Moufti, M., Broad accommodation of rift-related extension recorded by dyke intrusion in Saudi Arabia: Nature Geoscience, 3, 705-712, 2010.

** The pdf files of our publications are available upon request.